Cellular contributions to ictal population signals

Lauren A. Lau[1], Zhuoyang Zhao[1], Stephen N. Gomperts,[1] Kevin J. Staley[1] and Kyle P. Lillis[1]

Abstract

The amplitude of ictal activity is a defining feature of epileptic seizures, but the determinants of this amplitude have not been studied. Pathological synchronization of neuronal activity is assumed to be the main driver of increased ictal amplitudes. However, cell intrinsic changes that drive pathological neuronal discharges may also contribute to ictal amplitude. Clinically, ictal amplitudes are measured electrographically (using e.g. EEG, ECoG, and depth electrodes), but these methods do not enable the assessment of the contributions of the amplitudes of individual neurons as well as synchronization to the amplitude of the ictal signal. We therefore measured ictal population activity by recording both electrographic local field potentials (LFP) and neuronal calcium levels, the latter measured using optical imaging of neuronal transgenic calcium-sensitive fluorophores. Spontaneous seizure activity was first assessed in an awake, behaving mouse model of focal cortical injury, using paired GCaMP6-based calcium imaging and LFP electrical recording. Spontaneous recurrent seizures were then measured in organotypic hippocampal slice cultures (OHSC), with a combination of GCaMP7 calcium imaging and LFP recordings. OHSC is an in vitro preparation in which all electrical and calcium signals could be unambiguously ascribed to the epileptic network. Population-averaged calcium activity was highly correlated with the time integral of electrographic field recordings, both in vivo and in vitro. We found that cell intrinsic changes were the largest contributor to the population signal during seizure onset. In other words, the network signal was not merely the summation of highly synchronous physiological activity, but that individual neurons were generating pathological discharges. During frank seizure, individual neurons continued to generate pathological activity, which also became highly synchronized. Interestingly, recruitment of newly active neurons accounted for only a small fraction of synchronous activity, particularly in vivo, revealing that network synchrony was largely due to reactivation of the same population of neurons.

Author affiliations:

1 Massachusetts General Hospital, Department of Neurology, Boston, Massachusetts 02114, Harvard Medical School, Boston, Massachusetts 02115.

Correspondence to: Kyle P. Lillis

114 16th Street, Charlestown Navy Yard, MA 02129

klillis@mgh.harvard.edu

Running title: Cellular contributions to ictal signals

Keywords: epilepsy; seizure; calcium imaging; local field potential

Abbreviations: DIV = Days in Vitro; GECI = Genetically Encoded Calcium Indicator; GRIN = Gradient-Index; ICV = Intracerebral-ventricular; LFP = Local Field Potential; MUA = Multi-Unit Activity; OHSC = Organotypic Hippocampal Slice Culture; P = Postnatal Day; PDS = Paroxysmal Depolarizing Shift; ROI = Region of Interest; STD = Standard Deviation

Introduction

The amplitude of paroxysmal ictal activity is a defining feature of epileptic seizures. Although low-amplitude seizures occur, for example in infantile spasms (Panzica et al., 1999), this is the exception. The rule is that seizure activity is recognizable in electroencephalographic recordings in large part because of the distinguishing increase in EEG amplitude during seizure activity (Engel, 1984; Noachtar and Remi, 2009). Automatic seizure detection systems utilize the power or energy of the ictal signal, which are proportional to the amplitude, as an important (but not the solitary) feature of seizure activity (Gotman, 1985; Greene et al., 2008). However, the determinants of this unique increase in amplitude have not been studied.

The EEG signal is a nonlinear summation of the activity of the neurons and glia in the underlying cortex (Schevon et al., 2019; Tao et al., 2007). A well-known contributor to the ictal signal is the neuronal paroxysmal depolarizing shift (PDS) in the neuronal membrane potential, which lasts 100s of milliseconds and is typically 50 mV in amplitude (Kandel and Spencer, 1961a; Matsumoto and Marsan, 1964). However, lower-amplitude synaptic activity also contributes to the ictal EEG, including the barrages of excitatory postsynaptic potentials that are thought to trigger the PDS and propagate seizure activity (Buzsáki et al., 2012; Schevon et al., 2012).

In addition to these high and low amplitude cell-autonomous contributions to ictal seizure amplitude, another seizure characteristic, increased synchrony, increases the amplitude of the seizure signal. Scalp EEG has long been recognized to report a spatial average of underlying cortical activity. Only activity that is synchronous across the reported cortical volume is of sufficient amplitude to be recognizable in the scalp EEG (Delucchi et al., 1962). High-amplitude epileptiform EEG activity has therefore been considered to represent more highly synchronous activity of cortical neurons (Tao et al., 2007). This has been confirmed in recordings from cortical microelectrode arrays (Schevon et al., 2012). Increases in amplitude as a consequence of synchrony can arise from the recurrent activation of neurons, or from the recruitment of new populations of neurons into synchronous activity (Merricks et al., 2021).

There are thus 4 defined contributors to the amplitude of the EEG: low amplitude and high amplitude cell autonomous activity, and the synchrony of that activity arising from either recurrent neuronal activation or recruitment of new populations into the seizure. Electrophysiological

methods are not ideal to parse the individual contributions of these elements to ictal amplitude because recordings of population activity are not readily linked to the electrical activity of individual neurons. Current source density measures, coupled with estimates of the voltage drops generated by these currents as they flow through the extracellular space, require complex models (Baillet et al., 2001; Hallez et al., 2007). Microelectrode array recordings can identify spiking in nearby, individual neurons during baseline activity, but arguably not during seizures (Merricks et al., 2021). These models cannot unambiguously answer the question: what are the determinants of the increased amplitude of ictal activity? We therefore turned to optical measures of neuronal activity to assess their contributions to ictal amplitude.

Calcium imaging is a convenient surrogate measure of neuronal electrical activity, as calcium flux through voltage-gated calcium channels during action potential increases cytoplasmic calcium from ~40nm to >10µM (Helmchen et al., 1997), producing a signal that is easily detected with calcium-sensitive fluorophores. The kinetics of calcium-sensitive fluorophores have rapidly improved in the past decade, with the latest iterations reporting a half-rise time of 7.1ms (Zhang et al., 2020). However, the decay kinetics remain slow relative to electrical activity, making it challenging to resolve high frequency spike timing in individual neurons. Recent work with novel, transparent graphene electrodes, demonstrated the utility of simultaneously recording, during seizure, electrophysiological signals (with high temporal resolution) and calcium signals (with high spatial resolution and genetic targetability), but stopped short of analyzing cellular signals (Driscoll et al., 2021).

Here, spontaneous seizure activity was recorded from the hippocampus in awake, behaving mice using microendoscope calcium imaging and LFP in a model of focal cortical injury (where seizures were observed following cortical aspiration in the seizure susceptible APP/PS1 mouse (Reyes-Marin and Nunez, 2017)). We also performed multimodal recordings in a reduced, chronically epileptic preparation, the organotypic hippocampal slice culture (OHSC). With this preparation, we can record with cellular resolution from the entire epileptic network (Lau et al., 2021) allowing us to study contributions to the ictal signal that could be unambiguously ascribed to the seizure focus. We developed a novel method to quantify the relative contribution of inter-cellular and intra-cellular sources (i.e. both pathological synchronization and cell intrinsic pathological discharges) to the overall ictal signal. Seizure onset was largely marked by cell autonomous

changes, with a minority of the signal coming from network synchrony. Interestingly, we found that nearly the entire network was recruited (i.e. active at least once) during seizure onset in OHSC, and the transition to frank seizure was driven by synchronous activation of previously recruited cells. While a smaller total percentage of neurons were recruited during in vivo seizure (~60% of identified neurons recruited per seizure), new recruitment accounted for less than 1% of the overall increase in population signal during seizure. The observed differences in total recruitment may be due to differences in the models (reduced in vitro preparation versus whole brain) or in recruitment dynamics for initiation versus propagation. This work provides a framework for the careful quantification of the underlying sources to population signals that can be applied in multiple models and both physiological and pathological brain states.

Materials and methods

All animal protocols were approved by the Massachusetts General Hospital Subcommittee on Research and Animal Care.

In Vivo Virus Injection

Virus injection was performed as previously described (Zhou et al., 2019). Adult APP1/PS1 mice were anesthetized under isoflurane, with 4% for induction and 1.5 – 2.0% for maintenance. The animal was head-fixed on a stereotaxic frame and given a short incision on the head skin (under a dissection microscope). Then the cut was further extended into areas of the bregma and the cerebellum. The underneath soft tissue was cleared to expose the skull. A position in the right hemisphere for hippocampal CA1 at anterior-posterior (AP) -2.10 mm and medial-lateral (ML) 1.65 mm was marked on the skull for virus injection. The spot was drilled down gradually to achieve thinning of its covering bone, after which the bone was removed to expose the brain surface. 1 μl of AAV1-hSyn-GCaMP6f virus solution (with a titer of ~ 1 $x10^{13}$/ml) was injected at the spot (dorsal-ventral (DV) -1.40 mm). A suture was performed to close the cut. After the virus injection, the animal was returned to the housing facility, and was allowed to recover for 2 weeks.

Endoscope and GRIN Lens Implantation Surgery

Surgery was performed as previously described (Zhou et al., 2019). The animal was anesthetized under isoflurane, with 4% for induction and 1.5 – 2.0% for maintenance. The animal was head-fixed on a stereotaxic frame and given a short incision on the head skin (under a dissection microscope). Then the cut was further extended into areas of the bregma and the cerebellum. The underneath soft tissue was cleared to expose the skull. Two positions were marked on the skull for implantations of a lens (for calcium imaging) and an electrophysiology probe, AP -2.1 mm and ML -1.5 from Bregma, and AP -2.8 and ML 2.6, respectively. The two spots were drilled down gradually to achieve thinning of their covering bones. Then several metal screws were installed distributivity on the skull except for the areas for the implantations. One screw in the cerebellum area had a short piece of silver wire attached to itself, to be used later as the grounding wire. After removal of the thinned bones at the implantation sites, the brain was exposed at the pial surface for electrophysiology. To prepare for imaging lens implantation, the cortex above the hippocampal CA1 region was carefully removed using a vacuuming needle. A gradient-index (GRIN) lens with 4mm in length and 1mm in diameter (Inscopix) was implanted vertically and lowered until right above the CA1 region. An in-house custom-made adjustable electrophysiology-probe consisting of 7 stereotrodes was then tilted to a 36/39 degrees, dorsal-ventral -1.7mm from brain surface, and implanted to a reasonable depth (for ease of later adjustment during electrophysiology signal acquisition) to sample local field potential and unit activity in the vicinity of the imaged CA1 neuronal population. The silver grounding wire was then soldered to the probe's corresponding grounding pins. Dental cement was applied onto the skull, embedding the metal screws and surrounding the GRIN lens and electrophysiology-probe, to make everything firmly stabilized. After surgery, the animal was returned to the housing facility, and allowed to recover. 3 weeks later (with the animal under the same procedure of anesthesia), a baseplate (Inscopix) was placed above the implanted GRIN lens at an appropriate height, and position-secured by dental cement.

In Vivo Calcium Imaging and Electrophysiology Recordings

With a miniscope (Inscopix) mounted onto the baseplate, and a headstage pre-amplifier (Neuralynx) connected to the implanted electrophysiology-probe, the animal was allowed to habituate in its home cage for 30 minutes. After habituation, simultaneous calcium imaging and

electrophysiology recordings were acquired, as described in our previous work (Zhou et al., 2019). Calcium was recorded with the Inscopix imaging system and electrophysiology acquired with a Neuralynx system, with one TTL pulse per calcium imaging frame to sync the two. Calcium imaging was acquired at 20 Hz. Three 10-minute-long imaging sessions were performed during a period of quiet wakefulness, with a 5-minute off period between to prevent the bleaching of the GCaMP6f signal. The electrophysiology signal was sampled at 32 kHz (filtered at 0.5 - 900 Hz) and was acquired continuously throughout the duration of the experiment. To compare calcium signal and electrophysiology, the signal was first filtered for multi-unit activity. It was then rectified and down-sampled to match the imaging rate. Finally, the signal was convolved with a half-life decay of 142 ms to match the decay kinetics of GCaMP6f (Chen et al., 2013).

Organotypic Hippocampal Slice Culture (OHSC) Preparation

Newborn DLX-cre mouse pups (Post-natal day (P) 1-2) received intracerebroventicular (ICV) injections of AAV-hSyn-GCaMP7f to express GCaMP7f pan-neuronally. Organotypic slice cultures were prepared from P6-P8 DLX-cre mice of either sex using the membrane insert technique (Stoppini et al., 1991), as described previously (Lau et al., 2021). Briefly, isolated hippocampi were cut into 400 μm slices on a McIlwain tissue chopper (Mickle Laboratory Engineering). Slices were then transferred to membrane inserts (Millipore) and placed into six-well plates. Cultures were incubated in a custom-designed imaging system at 5% CO2, 36°C in 1 mL of Neurobasal-A growth medium supplemented with 2% B27, 500 μM GlutaMAX, and 0.03 mg/ml gentamycin (all from Invitrogen).

OHSC Chronic Calcium Imaging

On the day of slice culture preparation, slices were transferred to the custom imaging system, an inverted microscope constructed inside of a CO2 incubator (Jacob et al., 2019; Lau et al., 2021). The microscope comprises an Olympus XL Fluor 4X objective (0.28 NA), emission filters at 525/50 and 630/75 nm (Chroma) for GCaMP and tdTomato, respectively, filter wheel (Thorlabs), blue and green LED excitation sources (Sutter Instruments) and a sCMOS camera (pco.edge). Slices were positioned using a motorized stage, equipped with a multiwell plate mount. Slice cultures remained mounted in the imaging system for the duration of the experiment with media exchange happening via a computer-controlled multi-channel perfusion pump. Slices were imaged

every 6 hours to obtain an 85-second time series of green fluorescence at 35 Hz to record the spatiotemporal dynamics of calcium activity.

OHSC Electrophysiology

In some experiments, imaging was paired with electrical recordings of the extracellular field potential. Membrane inserts were prepared with a tungsten recording electrode (tungsten wire de-insulated at the tip) and slice cultures were grown directly on top of the recording electrode. Data was collected at 1 KHz using a DC amplifier (Warner Instruments) at 100X gain with a 0.1 KHz filter. To compare calcium signal and the LFP, the signal was rectified and down-sampled (by averaging the absolute value of a window of 28 frames). This signal was then convolved with a half-life decay of 520 ms to match the decay kinetics of GCaMP7f (Dana et al., 2019).

Pre-processing of Calcium Signal

In vivo: Neuronal regions of interest (ROI) were identified with the Fiji plugin TrackMate (Schindelin et al., 2012), using a Laplacian of Gaussian filter to identify GCaMP+ neuronal cell bodies. TrackMate was used to follow the position of the same ROI over time and correct for motion artifact. The mean pixel intensity was extracted from the somatic ROI and a surrounding anulus ROI of neuropil. The calcium traces were normalized as Δf/f, and then corrected for neuropil contamination as:

$$\frac{\Delta f}{f} corrected = \frac{\Delta f}{f}\ soma - \left(0.95 * \frac{\Delta f}{f}\ neuropil\right)$$

The weighing factor 0.95 was determined empirically to maximize the subtraction while avoiding over-correction.

OHSC: GCaMP+ cells were identified from a standard deviation projection (STD) of the high-resolution calcium recordings, which highlights pixels with dynamic signal. The Fiji plugin TrackMate (Schindelin et al., 2012) was used to automatically select ROIs corresponding to the soma of active cells from the STD projection. The mean pixel intensity was extracted from the somatic ROI and a surrounding anulus ROI of neuropil. Somatic signal was corrected for neuropil contamination as:

$$F\ corrected = F\ soma - (0.8 * F\ neuropil)$$

As above, the weighing factor 0.8 was determined empirically to maximize the subtraction while avoiding over-correction. In a subset of neurons, the somatic and neuropil ROIs were hand drawn (Supplemental Figure 3) to allow for neuropil contamination correction without a weighing factor (*F corrected = F soma – F neuropil*). F corrected was normalized as Δf/f, as described previously (Lau et al., 2021).

Separation of Subthreshold and Active States

The calcium signal of neurons can exist in two states: subthreshold and active. We developed here an automated method for separating these 2 states, by defining a threshold value calculated from a period of baseline inter-ictal activity.

In vivo: We first needed to identify a window of baseline activity (i.e. without seizure or epileptiform activity). This was done on a cell-by-cell basis using the absolute value of individual calcium traces high-pass filtered at 0.2 Hz to isolate periods without high-amplitude calcium transients. Threshold was then calculated as median + 2.5 standard deviations from the entire baseline period for each neuron. This strategy for defining threshold was selected by optimizing the detection of high-amplitude calcium transients (while minimizing false positives) in a sub-population of randomly selected cells. The thresholding process was then applied to the entire neuronal population in an automated fashion.

OHSC: A baseline window (without seizure or epileptiform activity) was identified in each seizure recording from the mean Δf/f trace. OHSC have inter-ictal periods of relative quiescence in all neurons, thus the same baseline window was used to calculate threshold in all neurons. Threshold was set as mean + 3 standard deviations on a cell-by-cell basis. Similar to above, the optimal thresholding strategy was determined empirically in a subset of randomly chosen neurons before being applied to all neurons in an automated process.

All analyses were performed in ImageJ (Fiji) and Matlab.

Quantification of Calcium Sources

The mean population calcium signal (mean Δf/f) can be calculated from 3 variable: Active fraction (fraction of neurons greater than threshold), Subthreshold [Ca^{+2}] (mean calcium amplitude of subthreshold neurons), and Active [Ca^{+2}] (mean calcium amplitude of active neurons):

$$Mean\frac{\Delta f}{f} =$$

$$\left(Subthreshold[Ca^{+2}] * \left(1 - \frac{\#\ active\ neurons}{total\ \#\ neurons}\right)\right) + \left(Active[Ca^{+2}] * \frac{\#\ active\ neurons}{total\ \#\ neurons}\right)$$

We can modify this equation to calculate how each variable contributes to the population signal compared to the baseline (inter-ictal) condition as:

$$Mean\frac{\Delta f}{f} =$$

$$\left(Subthr[Ca^{+2}]_B * (1 - fr.act) * \frac{Subthr[Ca^{+2}]}{Subthr[Ca^{+2}]_B}\right) + \left(Act[Ca^{+2}]_B * fr.act * \frac{Act[Ca^{+2}]}{Act[Ca^{+2}]_B}\right)$$

Where:

$Subthr[Ca^{+2}]_B$	= mean subthreshold baseline calcium amplitude
$Act[Ca^{+2}]_B$	= mean active baseline calcium amplitude
$fr.act$	= fraction active $\left(\frac{\#\ active\ neurons}{total\ \#\ neurons}\right)$

From this equation we can isolate the fraction of the increase that comes from synchronous activity (i.e. the fraction active) as:

$$Fraction\ synchrony =$$

$$\frac{\left(Subthr[Ca^{+2}]_B * (1 - fr.act)\right) + (Act[Ca^{+2}]_B * fr.act)}{Mean\ \frac{\Delta f}{f}}$$

Synchronous activity can be further separated as recruitment (first activation) or reactivation:

$$Fraction\ recruitment = \frac{(Act[Ca^{+2}]_B * fr.1st\ act)}{Mean\ \frac{\Delta f}{f}}$$

$$Fraction\ reactivation =$$

$$\frac{\left(Subthr[Ca^{+2}]_B * (1 - fr.act)\right) + (Act[Ca^{+2}]_B * (fr.act - fr.1st\ act))}{Mean\ \frac{\Delta f}{f}}$$

The remaining increase in the population signal is due to changes in the amplitude of the calcium signal of both the subthreshold ($Subthr[Ca^{+2}]$) and active ($Act[Ca^{+2}]$) states. These can be isolated as:

$$Fraction\ subthreshold\ amplitude =$$

$$\frac{\left(Subthr[Ca^{+2}]_B * (1 - fr.act) * \frac{Subthr[Ca^{+2}]}{Subthr[Ca^{+2}]_B}\right) - \left(Subthr[Ca^{+2}]_B * (1 - fr.act)\right)}{\left(Mean\ \frac{\Delta f}{f}\right) - \left(Act[Ca^{+2}]_B * fr.act * \frac{Act[Ca^{+2}]}{Act[Ca^{+2}]_B}\right)}$$

$$Fraction\ active\ amplitude =$$

$$\frac{\left(Act[Ca^{+2}]_B * fr.act * \frac{Act[Ca^{+2}]}{Act[Ca^{+2}]_B}\right) - (Act[Ca^{+2}]_B * fr.act)}{\left(Mean\ \frac{\Delta f}{f}\right) - \left(Subthr[Ca^{+2}]_B * (1 - fr.act) * \frac{Subthr[Ca^{+2}]}{Subthr[Ca^{+2}]_B}\right)}$$

Data availability

Data generated from this study is available upon reasonable request from the corresponding author.

Results

Genetically encoded calcium indicators (GECIs) to image seizure activity

Population level measures, such as EEG, are often used to describe seizure activity. However, these techniques do not capture the contributions of individual neurons to the network signal. Calcium imaging provides a way to record the activity of hundreds of neurons at a time and bridge the gap between single neuron and network activity. We first recorded neuronal resolution calcium during spontaneous seizures in awake, behaving animals, using a miniaturized fluorescence microscope and gradient refractive index (GRIN) lens in APP1/PS1 mice. APP/PS1 are double transgenic mice expressing mouse/human amyloid precursor protein and mutant human presenilin. These mutations are associated with early-onset Alzheimer's (Jankowsky et al., 2004), and have been shown to have an increased seizure susceptibility (Reyes-Marin and Nunez, 2017). In our experience, these mice will occasionally develop spontaneous seizures after a cortical aspiration injury. In this study, we recorded only from mice with non-convulsive seizures due to the limitation in imaging during convulsive seizures. Endoscopic calcium imaging was thus performed during seizures in the CA1 of awake, behaving APP/PS1 mice that had an acute cortical injury due to cortical aspiration/GRIN lens implantation (Figure 1A). Imaging of neuronal calcium was done with the genetically encoded calcium indicator (GECI) syn-GCaMP6f and was paired with recording of the local field potential (LFP) from a 7-channel linear probe sampling the nearby cortical and hippocampal areas. Seizures were defined as periods of high amplitude calcium events lasting >10 seconds, that coincided with increased amplitude in at least 1 channel of the LFP (Figure 1C). Rarely, seizures were observed where the increased amplitude in calcium was apparent tens of seconds earlier than the increased amplitude in the LFP. These seizures were analyzed as a separate class of Type II seizures (Supplemental Figure 6). Seizure onset was defined as the period of relatively lower amplitude activity when the population calcium could first be distinguished from baseline until the transition to frank seizure (marked by a local maximum in the population calcium slope). To capture whole network calcium during recurrent seizures, we also performed syn-GCaMP7f based calcium imaging in the organotypic hippocampal slice culture (OHSC) model (Figure 1B), which generates spontaneous seizures approximately 1-week post-

slicing injury (Berdichevsky et al., 2012) (Figure 1D). Due to the reduced size of the OHSC, the entire network can be sampled, allowing for the differentiation of activity in the seizure focus versus propagated activity. Both in vivo and in vitro, the calcium signal from hundreds of individual neurons was extracted from their somata (Figure 1E-F), which were identified using a Laplacian of Gaussian filter in the TrackMate plugin for ImageJ (Lau et al., 2021; Tinevez et al., 2017). The single cell calcium trace was corrected for neuropil contamination and normalized as $\Delta f/f$ (see Methods).

We found a high correlation between the population calcium activity and electrophysiology, both in vivo and in vitro. To compare the two modalities in vivo, we transformed the LFP by filtering for multiunit activity (MUA), rectifying, and down-sampling the data to 20 Hz (to match the imaging rate). After convolving with decay kinetics of GCaMP6f, we found a correlation of 0.7-0.84 between mean population calcium and the MUA activity, with the highest correlation occurring in the channel closest to the site of imaging (Supplemental Figure 1). We similarly transformed the LFP data recorded in vitro (Supplemental Figure 2) and found a correlation of 0.96 between the calcium signal and electrophysiology. The comparatively lower correlation between population calcium and MUA activity observed in vivo is likely due to the high number of unsampled neurons (i.e. neurons outside of the field of view) that contribute to the electrical activity in vivo. Overall, the high correlation in population calcium activity and the local field potential motivated our approach to use neuronal resolution calcium imaging to understand the contributions of individual neurons to epileptic network activity.

Calcium imaging to dissect population activity

The calcium signal of an individual neuron can be separated into 2 states: subthreshold and active. The subthreshold state is characterized by relatively stable, lower amplitude calcium that is consistent with physiological activity. Individual neurons may still be firing at low rates (<2 Hz) in the subthreshold state. Neurons may enter the active state (characterized by higher amplitude calcium) due to increased firing (allowing the calcium influx from individual action potentials to sum) or paroxysmal depolarizing shifts. In the inter-ictal period, active states often coincide with epileptiform activity. However, individual neurons may enter the active state without a corresponding network event. We designed a thresholding strategy to define the two states on a cell-by-cell basis (see Methods).

The fraction of active neurons was used as a measure of network synchrony. Synchrony could be further separated into recruitment (i.e. first activation) and reactivation (Figure 2D). Recruitment was based on each seizure event, such that the first time a neuron was in the active state in the onset/ictal window was considered the recruitment point. Each neuron could only be recruited once per seizure, and activity prior to seizure onset did not inform recruitment. In addition to changes in synchrony, there are also changes in the amplitude of the calcium signal (Figure 2A). The ΔF/F amplitude of individual neurons can evolve for both the active and subthreshold states. Together, these changes across individual neurons underly the population level signal (Figure 2B-D).

Network Synchrony during Seizure

To precisely quantify synchronous activity, neurons were separated as active or subthreshold at each time point (Figure 3). The instantaneous fraction of active neurons was used as our measure of synchrony (where fraction active = active neurons / total GCaMP+ population, in each time frame of either 28 ms (OHSC) or 50 ms (in vivo)). During baseline interictal activity, the mean fraction active was very low (0.2% ± 0.003, n = 82 recordings OHSC; 0.49% ± 0.08, n = 3 recordings in vivo). Across the same baseline period, 47.0% ± 0.6 (OHSC) and 7.2% ± 2.2 (in vivo) of neurons are active (above threshold) at least once, revealing low levels of asynchronous activity inter-ictally. The time-averaged fraction of co-activating cells increased during seizure onset (Figure 3A and B, mean percentage active 6.7% ± 0.6, n = 82 seizures in OHSC; Figure 3F and G, mean percentage active 8.2% ± 2.2, n = 5 seizures in vivo). Increased synchrony was even more pronounced during ictal activity (mean percentage active: 47.1% ± 1.9, over the first 10 seconds of seizure activity in OHSC; 20.0% ± 4.2 over entire ictal period in vivo). The percent active at each time point is calculated independently, and different neurons contribute to network synchrony point-to-point.

Recruitment was defined as the first threshold crossing during onset or subsequent seizure. New recruitment accounted for 32.2% ± 2.4 and 0.4% ± 0.2 of the total active fractions during onset and frank seizure in OHSC, (Figure 3D and E), with the remaining activity coming from re-activation. In vivo, new recruitment constitutes 2.7% ± 1.8 and 0.4% ± 0.2 of the total active fractions during onset and ictal activity (Figure 3F and G). The rate of new recruitment in OHSC was 32.5% ± 2.3 of total network recruited per second during onset and 2.0% ± 0.2 during ictus

(Fig 3C and D); while recruitment in vivo was much slower and occurred at a rate of 1.3% ± 0.01 (onset) and 1.0% ± 0.01 (ictal) (Figure 3H and I). In total, 78.6% ± 2.0 of neurons were recruited during seizure onset in OHSC, with the remaining 21.0% ± 2.0 of the neuronal population recruited during seizure, for a total cumulative recruitment of 99.6% ± 0.1 (Figure 3E). This reveals that the transition to frank seizure is largely due to synchronous activation of previously recruited neuronal populations in the organotypic hippocampal slice culture. In vivo, 23.7% ± 6.3 of neurons were recruited during seizure onset and 39.5% ± 6.0 during the ictal period, for a total cumulative recruitment of 63.2% ± 11.5 (Figure 3J). This lower total recruitment may be due to differences in the models (in vitro versus in vivo) or may reflect lower total recruitment occurring outside of the seizure focus.

Dynamics of the Intra-cellular Calcium Amplitude

In addition to the changes in synchronous activity, there are cell autonomous changes that occur during seizure that are reflected in the amplitude of the calcium signal in individual neurons. We can first consider the subthreshold state. Prior to seizure onset, neurons display a relatively stable subthreshold calcium amplitude. The baseline subthreshold calcium amplitude (Subthr $[Ca^{+2}]_B$) was calculated for each neuron by averaging the subthreshold Δf/f values during a window of interictal activity preceding seizure onset. This interictal period ranged from 11-56 seconds, depending on how much pre-seizure baseline activity was captured. To quantify the change in subthreshold amplitude, subthreshold calcium was normalized by Subthr $[Ca^{+2}]_B$ over time (Figure 4C). On average, the fold increase of the subthreshold calcium amplitude during seizure onset was 1.36 ± 0.02 (n = 82 seizures) in OHSC, and 1.68 ± 0.21 (n = 5 seizures) in vivo (Figure 4C and D). During frank seizure, the average fold increase in calcium amplitude was 2.03 ± 0.02 in OHSC, and 1.80 ± 0.42 in vivo (Figure 4C and E). While, by definition, neurons are below threshold at all points when they are included in the subthreshold population, on average the calcium amplitude is significantly increased during seizure onset ($p < 0.001$ OHSC; $p = 0.01$ in vivo, paired t-test) and ictus ($p < 0.001$ OHSC; $p = 0.01$ in vivo, paired t-test). To address the possibility of neuropil contamination driving this increase, we hand drew the regions of interest in a subset of neurons in OHSC (Supplemental Figure 3A). In this case, high fidelity neuropil subtraction can be performed (see Methods) and the increased subthreshold amplitude persists ($p = 0.003$ and $p < 0.001$, for onset and ictus respectively). Due to the sustained nature of the increase, sparse firing is unlikely

to account for the increase. Rather we predict that the subthreshold increase in calcium is due to intra-cellular calcium influx that is independent from neuronal firing, perhaps through low voltage activated calcium channels.

During seizure, the calcium amplitude of individual neurons also increases for the active state. As for the subthreshold state, a baseline active calcium amplitude (Act $[Ca^{+2}]_B$) was calculated for each neuron by averaging above threshold values from a period of inter-ictal activity. There were a subset of neurons in OHSC that were never in the active state during the inter-ictal window, and therefore had no values from which to calculate Act $[Ca^{+2}]_B$. In this case, Act $[Ca^{+2}]_B$ was estimated by using the first active amplitude value during seizure onset. On average, this estimated Act $[Ca^{+2}]_B$ was 11.1% ± 0.5 (n = 52) larger than the Act $[Ca^{+2}]_B$ from neurons within the same recording where the true active baseline amplitude could be calculated (Supplemental Figure 4A-C). Similarly, if we compare the Act $[Ca^{+2}]_B$ and first Act $[Ca^{+2}]$ during seizure onset from the same population of neurons, the first Act $[Ca^{+2}]$ was 6.0% ± 0.2 larger (n = 52, Supplemental Figure 4D). This suggests that the processes which drive the increase in active amplitudes begin early during seizure onset. On average, the fold increase of the active calcium amplitude during seizure onset was 1.08 ± 0.006 in OHSC (n = 82 seizures; $p < 0.001$ paired t-test compared to inter-ictal amplitude), and 1.20 ± 0.13 in vivo (n = 5 seizures; $p = 0.09$) (Figure 4C-H). During frank seizure, the average fold increase in active calcium amplitude was 1.37 ± 0.02 in OHSC ($p < 0.001$), and 1.40 ± 0.17 in vivo ($p = 0.04$) (Figure 4C-H). The observed increase in calcium amplitude is present even when accounting for the slower decay kinetics of GCaMP (Supplemental Figure 5). This reveals that neurons do not enter a static “active” state, but rather, that intra-cellular perturbations allow for higher levels of calcium signal to occur during seizure (perhaps through pathologically high rates of firing or PDS).

How synchrony and calcium amplitude changes contribute to total seizure activity

With synchrony and intra-cellular calcium amplitude precisely imaged on the individual neuron scale, the relative contribution of each source to population means can be quantitatively calculated (Figure 5A). The fractional increase coming from synchronous activity can be separated into recruitment and re-activation (where re-activation is synchrony among neurons that have entered

the active state at least once before in the current seizure event). This equation can be applied at any time point and in any activity state, to calculate the relative contribution of each source to the population mean (Figure 5B and D). On average in OHSC, the increased population signal during seizure onset is 9.0% ± 0.8 recruitment, 17.3% ± 0.1 re-activation, 4.3% ± 0.5 active Ca^{+2} amplitude, and 69.4% ± 1.5 subthreshold Ca^{+2} amplitude (n = 82 seizures; Figure 5C). In vivo, the population mean during seizure onset is 0.2% ± 0.03 recruitment, 15.7% ± 3.5 re-activation, 17.1% ± 4.1 active Ca^{+2} amplitude, and 67.0% ± 7.6 subthreshold Ca^{+2} amplitude (n = 5 seizures; Figure 5E). This substantiates a new finding that the majority of the signal increase during seizure onset is due to changes in the amplitude of intra-cellular calcium in neurons while they are below activation threshold. In other words, there are widespread, low-level calcium increases during seizure onset. During frank seizure in OHSC, the population signal is 0.9% ± 0.1 recruitment, 46.5% ± 0.7 re-activation, 25.5% ± 1.2 active Ca^{+2} amplitude, and 27.1% ± 1.6 subthreshold Ca^{+2} amplitude (Figure 5C). The relative contribution from each source remained constant over the 2-week period when recurrent, spontaneous seizures were recorded in vitro (Supplemental Figure 6). In vivo, the ictal population signal is 0.07% ± 0.01 recruitment, 26.7% ± 4.4 re-activation, 31.3% ± 6.7 active Ca^{+2} amplitude, and 42.0% ± 11.1 subthreshold Ca^{+2} amplitude (Figure 5E). While intra-cellular amplitude changes are still a significant factor during frank seizure, the contribution of synchronous activity is greater during ictal activity, with high levels of sustained activity in previously recruited cells. Increased contribution from synchronous activation is particularly pronounced in the OHSC, which may suggest that synchrony is highest in the seizure focus (and relatively lower in regions of seizure propagation, which is likely to be the case for the *in vivo* recordings).

Discussion

The quantifiable clinical hallmark of an epileptic seizure is manifest as an increase in the amplitude of EEG, preceded by a period of buildup and followed by a postictal depression. However, it remains largely unknown what features of neuronal activity correspond to the ictal increase in EEG amplitude. Many prior studies have evaluated the intracellular correlates of ictal activity in vivo (Kandel and Spencer, 1961b; Matsumoto and Marsan, 1964) and in vitro (Rutecki and Yang, 1998;

Westbrook and Lothman, 1983). The high correlation of large-amplitude activity in individual neurons and high-amplitude EEG potentials during seizures has led to the idea that the amplitude of the ictal EEG is a consequence of summed neuronal activity (Tao et al., 2007). A requisite for summation is synchronous neuronal activity (Delucchi et al., 1962). However, how the amplitude of the activity of individual neurons and the synchrony of that activity between individual neurons each contribute to the amplitude of the population activity has not previously been addressed.

Here, we synchronously recorded somatic calcium transients and local field potentials throughout the transition from interictal activity to ictal onset and frank seizure. Our finding that cell intrinsic changes were the largest contributor to the increase in LFP amplitude associated with ictogenesis may initially seem counterintuitive. It seems natural that an expanded population of co-activating neurons, either via recruitment of additional neurons or increasing the synchrony of active neurons, would sum to create a higher amplitude electrical field. But, how does fast electrical activity in a single neuron sum to produce a large transient in a field potential? There at least two factors that effectively integrate, or lowpass filter, electrical activity from the soma. Firstly, approximately 97% of a pyramidal neurons surface area is dendrite (DeFelipe and Farinas, 1992; Mungai, 1967), which means that the vast majority of extracellular field recording comes from postsynaptic potentials (PSPs) resulting from somatic action potentials (Nunez and Srinivasan, 2006). Since PSPs are inherently slower than action potentials, and arrive asynchronously at different locations, the extracellular electric field they generate is temporally broad. Thus, multiple action potentials from a single neuron would produce PSPs that “pile up” creating an integrated signal in the LFP, ECoG, and EEG. Further contributing to this effect is the spatial lowpass filtering that occurs in the brain, cerebrospinal fluid, and, in the case of scalp EEG, bone and skin tissue between the neuronal membrane and the electrode recording (Bedard et al., 2006).

Calcium imaging is an imperfect proxy for neuronal electrical activity. Although intracellular calcium transients comprise a lowpass filtered version of neuronal spiking (similar to field potential), the GCaMP7f indicators used here have a half-decay time constant of 270ms which corresponds to a cutoff frequency of approximately 1Hz (Dana et al., 2019), which is substantially lower than that provided by extracellular electrical recordings. While it would be ideal to use voltage-sensitive fluorophores to simultaneously record voltage in a large population of soma and dendrites, current fluorophores and imaging modalities limit the ability to perform such an

experiment in slices or *in vivo*. Thus, calcium imaging provides the only current means by which to sum the activity of individual members of a seizing neural population, particularly *in vivo*.

In vivo experiments are further complicated by the fact that spontaneous seizures in an intact animal are highly unlikely to originate at the site of imaging. Without comprehensive recordings, it is impossible to determine whether the activity imaged is in fact the seizure focus or propagation of a seizure that initiated elsewhere. Conversely, the organotypic slice culture represents a "focus only" model of seizure. Differences observed between the *in vivo* and *in vitro* preparations in the relative contributions of reactivation, recruitment, and cell-intrinsic activity to LFP amplitude may reflect differences in focal vs propagated ictogenesis.

In vivo, we were surprised to find that subthreshold calcium activity was the single largest contributor to population activity during both ictal onset and frank seizure. The area recorded may have been primarily an area into which the seizure propagated. During propagation, the gradual collapse of surround inhibition is a key feature (Prince and Wilder, 1967; Trevelyan and Schevon, 2013) and this would be primarily reflected in the amplitude of subthreshold calcium activity (Trevelyan and Schevon, 2013). To address this issue, we performed experiments in OHSC, in which the entire hippocampus can be considered to be within the focus, rather than an area of propagation (Lau et al., 2021). In this preparation, subthreshold calcium activity was the largest determinant of the amplitude of population activity during ictal onset. However, during frank seizure activity, the synchronous reactivation of neurons was the largest determinant of the amplitude of population activity. This supports the idea that in the focus, inhibition has failed during seizure activity (Lillis et al., 2012), so that subthreshold calcium activity is a relatively minor contributor to ictal amplitude. The failure of inhibition was also a requisite for the onset of seizure activity in our prior modeling studies of seizures in this preparation (Jacob et al., 2019).

It may be that the relative contribution of subthreshold calcium activity will prove to be a reliable biomarker of ictal activity within the focus vs. propagated ictal activity. A closely related feature that might be a more feasible biomarker is the fraction of neurons active during ictal activity (Figure 3). In the focus, the fraction of active cells is much higher than in the putative propagation areas recorded in vivo. However, this idea requires confirmation of the status of the in vivo recordings as being from propagated areas. It is also possible that inhibition is simply more robust in vivo as a consequence of the intact inputs from surrounding areas.

Funding

This work was supported by National Institute of Neurological Disorders and Stroke.

Competing interests

The authors report no competing interests.

References

Baillet, S., J.C. Mosher, and R.M. Leahy. 2001. Electromagnetic brain mapping. *IEEE Signal Processing Magazine*. 18:14-20.

Bedard, C., H. Kroger, and A. Destexhe. 2006. Model of low-pass filtering of local field potentials in brain tissue. *Phys Rev E Stat Nonlin Soft Matter Phys*. 73:051911.

Berdichevsky, Y., V. Dzhala, M. Mail, and K.J. Staley. 2012. Interictal spikes, seizures and ictal cell death are not necessary for post-traumatic epileptogenesis in vitro. *Neurobiol Dis*. 45:774-785.

Buzsáki, G., C.A. Anastassiou, and C. Koch. 2012. The origin of extracellular fields and currents--EEG, ECoG, LFP and spikes. *Nat Rev Neurosci*. 13:407-420.

Chen, T.W., T.J. Wardill, Y. Sun, S.R. Pulver, S.L. Renninger, A. Baohan, E.R. Schreiter, R.A. Kerr, M.B. Orger, V. Jayaraman, L.L. Looger, K. Svoboda, and D.S. Kim. 2013. Ultrasensitive fluorescent proteins for imaging neuronal activity. *Nature*. 499:295-300.

Dana, H., Y. Sun, B. Mohar, B.K. Hulse, A.M. Kerlin, J.P. Hasseman, G. Tsegaye, A. Tsang, A. Wong, R. Patel, J.J. Macklin, Y. Chen, A. Konnerth, V. Jayaraman, L.L. Looger, E.R. Schreiter, K. Svoboda, and D.S. Kim. 2019. High-performance calcium sensors for imaging activity in neuronal populations and microcompartments. *Nature methods*. 16:649-657.

DeFelipe, J., and I. Farinas. 1992. The pyramidal neuron of the cerebral cortex: morphological and chemical characteristics of the synaptic inputs. *Progress in neurobiology*. 39:563-607.

Delucchi, M.R., B. Garoutte, and R.B. Aird. 1962. The scalp as an electroencephalographic averager. *Electroencephalogr Clin Neurophysiol*. 14:191-196.

Driscoll, N., R.E. Rosch, B.B. Murphy, A. Ashourvan, R. Vishnubhotla, O.O. Dickens, A.T.C. Johnson, K.A. Davis, B. Litt, D.S. Bassett, H. Takano, and F. Vitale. 2021. Multimodal in vivo recording using transparent graphene microelectrodes illuminates spatiotemporal seizure dynamics at the microscale. *Commun Biol*. 4:136.

Engel, J., Jr. 1984. A practical guide for routine EEG studies in epilepsy. *J Clin Neurophysiol*. 1:109-142.

Gotman, J. 1985. Seizure recognition and analysis. *Electroencephalogr Clin Neurophysiol Suppl*. 37:133-145.

Greene, B.R., S. Faul, W.P. Marnane, G. Lightbody, I. Korotchikova, and G.B. Boylan. 2008. A comparison of quantitative EEG features for neonatal seizure detection. *Clin Neurophysiol*. 119:1248-1261.

Hallez, H., B. Vanrumste, R. Grech, J. Muscat, W. De Clercq, A. Vergult, Y. D'Asseler, K.P. Camilleri, S.G. Fabri, S. Van Huffel, and I. Lemahieu. 2007. Review on solving the forward problem in EEG source analysis. *J Neuroeng Rehabil*. 4:46.

Helmchen, F., J.G. Borst, and B. Sakmann. 1997. Calcium dynamics associated with a single action potential in a CNS presynaptic terminal. *Biophys J*. 72:1458-1471.

Jacob, T., K.P. Lillis, Z. Wang, W. Swiercz, N. Rahmati, and K.J. Staley. 2019. A Proposed Mechanism for Spontaneous Transitions between Interictal and Ictal Activity. *J Neurosci*. 39:557-575.

Jankowsky, J.L., D.J. Fadale, J. Anderson, G.M. Xu, V. Gonzales, N.A. Jenkins, N.G. Copeland, M.K. Lee, L.H. Younkin, S.L. Wagner, S.G. Younkin, and D.R. Borchelt. 2004. Mutant presenilins specifically elevate the levels of the 42 residue beta-amyloid peptide in vivo: evidence for augmentation of a 42-specific gamma secretase. *Hum Mol Genet*. 13:159-170.

Kandel, E.R., and W.A. Spencer. 1961a. Electrophysiology of hippocampal neurons. II. After-potentials and repetitive firing. *J Neurophysiol*. 24:243-259.

Kandel, E.R., and W.A. Spencer. 1961b. Excitation and inhibition of single pyramidal cells during hippocampal seizure. *Exp Neurol*. 4:162-179.

Lau, L.A., K.J. Staley, and K.P. Lillis. 2021. In vitro ictogenesis is stochastic at the single neuron level. *Brain*.

Lillis, K.P., M.A. Kramer, J. Mertz, K.J. Staley, and J.A. White. 2012. Pyramidal cells accumulate chloride at seizure onset. *Neurobiol Dis*. 47:358-366.

Matsumoto, H., and C.A. Marsan. 1964. Cortical Cellular Phenomena in Experimental Epilepsy: Ictal Manifestations. *Exp Neurol*. 9:305-326.

Merricks, E.M., E.H. Smith, R.G. Emerson, L.M. Bateman, G.M. McKhann, R.R. Goodman, S.A. Sheth, B. Greger, P.A. House, A.J. Trevelyan, and C.A. Schevon. 2021. Neuronal Firing and Waveform Alterations through Ictal Recruitment in Humans. *J Neurosci*. 41:766-779.

Mungai, J.M. 1967. Dendritic patterns in the somatic sensory cortex of the cat. *J Anat*. 101:403-418.

Noachtar, S., and J. Remi. 2009. The role of EEG in epilepsy: a critical review. *Epilepsy & behavior : E&B*. 15:22-33.

Nunez, P.L., and R. Srinivasan. 2006. Electric fields of the brain: the neurophysics of EEG. Oxford University Press, USA.

Panzica, F., S. Franceschetti, S. Binelli, L. Canafoglia, T. Granata, and G. Avanzini. 1999. Spectral properties of EEG fast activity ictal discharges associated with infantile spasms. *Clin Neurophysiol*. 110:593-603.

Prince, D.A., and B.J. Wilder. 1967. Control mechanisms in cortical epileptogenic foci. "Surround" inhibition. *Arch Neurol*. 16:194-202.

Reyes-Marin, K.E., and A. Nunez. 2017. Seizure susceptibility in the APP/PS1 mouse model of Alzheimer's disease and relationship with amyloid beta plaques. *Brain Res*. 1677:93-100.

Rutecki, P.A., and Y. Yang. 1998. Ictal epileptiform activity in the CA3 region of hippocampal slices produced by pilocarpine. *J Neurophysiol*. 79:3019-3029.

Schevon, C.A., S. Tobochnik, T. Eissa, E. Merricks, B. Gill, R.R. Parrish, L.M. Bateman, G.M. McKhann, R.G. Emerson, and A.J. Trevelyan. 2019. Multiscale recordings reveal the dynamic spatial structure of human seizures. *Neurobiol Dis*. 127:303-311.

Schevon, C.A., S.A. Weiss, G. McKhann, R.R. Goodman, R. Yuste, R.G. Emerson, and A.J. Trevelyan. 2012. Evidence of an inhibitory restraint of seizure activity in humans. *Nat Commun*. 3:1060.

Schindelin, J., I. Arganda-Carreras, E. Frise, V. Kaynig, M. Longair, T. Pietzsch, S. Preibisch, C. Rueden, S. Saalfeld, B. Schmid, J.Y. Tinevez, D.J. White, V. Hartenstein, K. Eliceiri, P. Tomancak, and A. Cardona. 2012. Fiji: an open-source platform for biological-image analysis. *Nat Methods*. 9:676-682.

Stoppini, L., P.A. Buchs, and D. Muller. 1991. A simple method for organotypic cultures of nervous tissue. *J Neurosci Methods*. 37:173-182.

Tao, J.X., M. Baldwin, S. Hawes-Ebersole, and J.S. Ebersole. 2007. Cortical substrates of scalp EEG epileptiform discharges. *J Clin Neurophysiol*. 24:96-100.

Tinevez, J.Y., N. Perry, J. Schindelin, G.M. Hoopes, G.D. Reynolds, E. Laplantine, S.Y. Bednarek, S.L. Shorte, and K.W. Eliceiri. 2017. TrackMate: An open and extensible platform for single-particle tracking. *Methods*. 115:80-90.

Trevelyan, A.J., and C.A. Schevon. 2013. How inhibition influences seizure propagation. *Neuropharmacology*. 69:45-54.

Westbrook, G.L., and E.W. Lothman. 1983. Cellular and synaptic basis of kainic acid-induced hippocampal epileptiform activity. *Brain Res*. 273:97-109.

Zhang, Y., M. Rozsa, D. Bushey, J. Zheng, D. Reep, G.J. Broussard, A. Tsang, G. Tsegaye, R. Patel, S. Narayan, J.X. Lim, R. Zhang, M.B. Ahrens, G.C. Turner, S.S.-H. Wang, K. Svoboda, W. Korff, E.R. Schreiter, J.P. Hasseman, I. Kolb, and L.L. Looger. 2020. jGCaMP8 Fast Genetically Encoded Calcium Indicators. *In* Janelia.

Zhou, H., K.R. Neville, N. Goldstein, S. Kabu, N. Kausar, R. Ye, T.T. Nguyen, N. Gelwan, B.T. Hyman, and S.N. Gomperts. 2019. Cholinergic modulation of hippocampal calcium activity across the sleep-wake cycle. *Elife*. 8.

Figure legends

Figure 1: Paired Calcium Imaging and Local Field Potential In Vivo and In Vitro. A) Representative image of standard deviation projection during syn-GCaMP6f calcium imaging in vivo. Scale bar = 100 μm. B) Representative image of standard deviation projection during syn-GCaMP67f calcium imaging in Organotypic Hippocampal Slice Culture (OHSC). Scale bar = 100 μm. C) Paired mean GCaMP6f Δf/f trace and 3 channels of local field potential (LFP) during seizure onset (pink) and ictal (red) activity, in vivo. D) Paired mean GCaMP7f Δf/f trace and local field potential (LFP) during seizure onset (pink) and ictal (red) activity, in OHSC. E) Raster plot of calcium signal of individual neurons from seizure in panel C. Colorbar = Δf/f. F) Raster plot of calcium signal of individual neurons from seizure in panel D. Colorbar = Δf/f.

Figure 2: Changes in Synchrony and Calcium Amplitude Underly Population Level Changes. A) Illustration of single cell calcium trace to demonstrate changes in frequency and amplitude of the active and inactive states. Phase of seizure indicated by colorbar. B) Example raster plot of calcium signal for 10 individual neurons during baseline activity C) Example network calcium during seizure. C1: Mean population calcium Δf/f. C2: raster of the calcium Δf/f of 10 individual neurons, phases of seizure indicated by colorbar as in (A). C3: Plot of mean active fraction over time. C4: Plot of the mean subthreshold [Ca^{+2}] amplitude over time. C5: Plot of the mean active [Ca^{+2}] amplitude over time. D) Plot of new recruitment and total cumulative recruitment, as a fraction of the total number of neurons.

Figure 3: Recruitment and Synchronous Activity. A) Example plot of fraction of active neurons (above threshold) over time during seizure in OHSC. Color represents fraction active that is new recruitment. B) Beeswarm plot of time-averaged fraction of active neurons during seizure onset and ictal period. Colorbar = mean recruitment/total fraction active. n = 82 seizures. C) Example plot of instantaneous recruitment (black) and cumulative recruitment (blue). D) Beeswarm plot of mean rate of recruitment (fraction of total network recruited per second) during onset and ictal periods E) Beeswarm plot of cumulative recruitment during onset, ictal and in total (onset + ictal) F) Example plot of fraction of active neurons (above threshold) over time during seizure in vivo. Color represents fraction active that is new recruitment. G) Beeswarm plot of time-averaged fraction of active neurons during seizure onset and ictal. Colorbar = mean recruitment/total fraction active. n = 5 in vivo seizures. H) Example plot of instantaneous recruitment (black) and cumulative recruitment (blue). I) Beeswarm plot of mean rate of recruitment (fraction of total network recruited per second) during onset and ictal periods J) Beeswarm plot of cumulative recruitment during onset, ictal and in total (onset + ictal).

Figure 4: Change in Calcium Amplitude. A) Top: example single cell calcium Δf/f from OHSC, with time points in the active state indicated by red circle. Bottom: Raster plot of the same calcium trace separated into subthreshold and active (above threshold). Colorbar = Δf/f. B) Example raster plot of the calcium signal of neurons across an entire network, separated into subthreshold and active. Black bar = baseline period. C) Example mean baseline normalized subthreshold amplitude over time of all neurons in OHSC. D) Beeswarm plot of time-averaged change in subthreshold amplitude during seizure onset and ictal period in OHSC. n = 82 seizures. E) Beeswarm plot of time-averaged change in subthreshold amplitude during seizure onset and ictal period in vivo. n = 5 seizures. F) Example mean baseline normalized active amplitude over time of all neurons in OHSC. G) Beeswarm plot of time-averaged change in active amplitude during seizure onset and ictal period in OHSC. H) Beeswarm plot of time-averaged change in active amplitude during seizure onset and ictal period in vivo.

Figure 5: Quantifying Sources of Increased Population Calcium Signal During Seizure. A) Equation for quantifying the sources of mean population calcium signal (compared to a baseline inter-ictal period). $[Ca^{+2}]_B$ = baseline calcium amplitude B) Example plot showing the sources of the population signal compared to baseline over time in OHSC; yellow = recruitment, red = synchronous activity, cyan = change in the active amplitude, and blue = change in the subthreshold amplitude. Scale bar = 0.01 Δf/f and 5 secs. C) Pie chart = mean percent of population increase from each source (recruitment, synchrony, active $[Ca^{+2}]$ amplitude, subthreshold $[Ca^{+2}]$ amplitude), n = 82 seizures. D) Example plot showing the sources of the population signal compared to baseline over time in vivo; yellow = recruitment, red = synchronous activity, cyan = change in the active amplitude, and blue = change in the subthreshold amplitude. Scale bar = 0.01 Δf/f and 5 secs. E) Pie chart = mean percent of population increase from each source (recruitment, synchrony, active $[Ca^{+2}]$ amplitude, subthreshold $[Ca^{+2}]$ amplitude), n = 5 seizures.

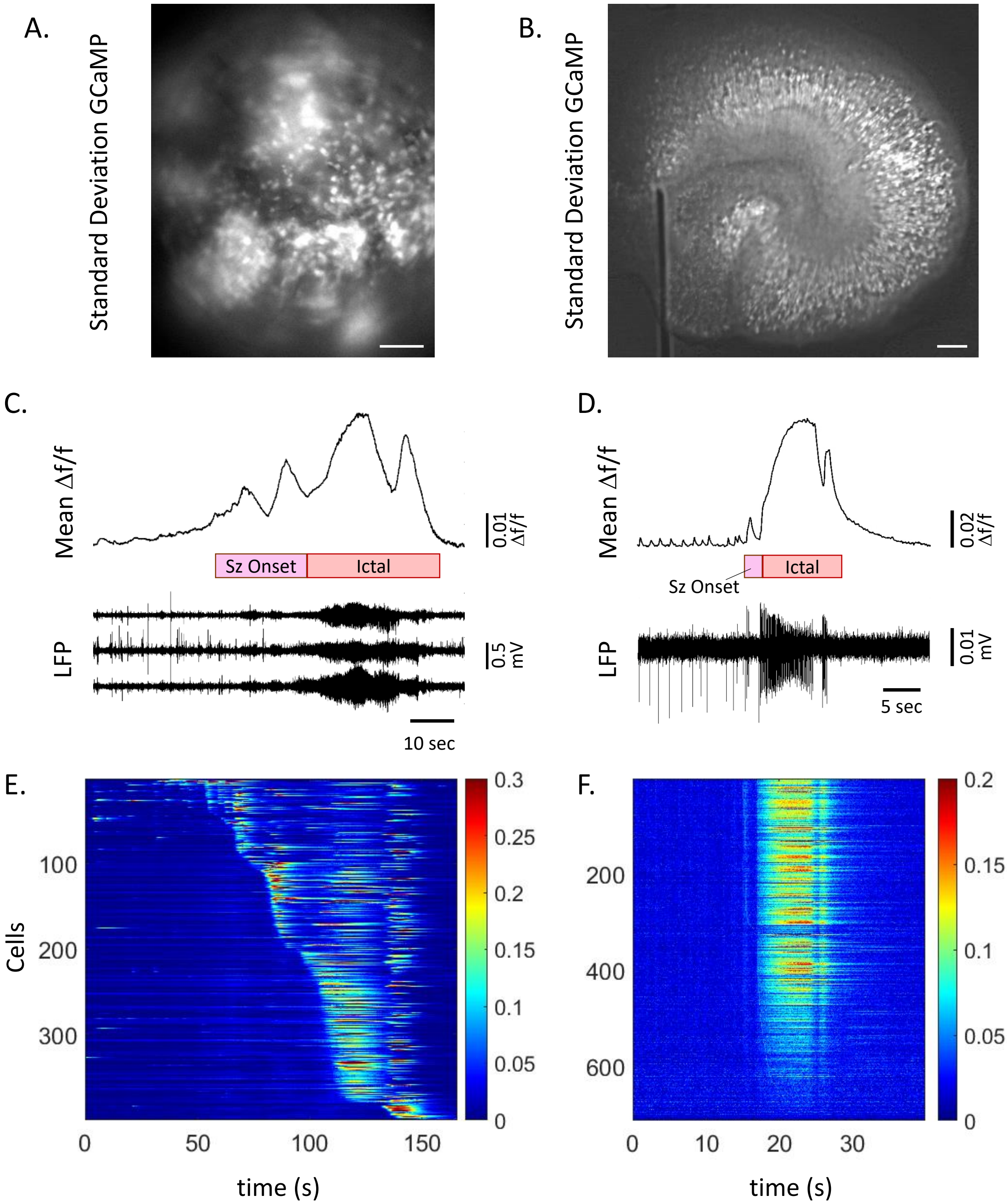
A.
Standard Deviation GCaMP
B.
Standard Deviation GCaMP
C.
Mean Δf/f
Sz Onset
Ictal
0.01 Δf/f
LFP
0.5 mV
10 sec
D.
Mean Δf/f
Ictal
Sz Onset
0.02 Δf/f
LFP
0.01 mV
5 sec
E.
Cells
100
200
300
0
50
100
150
time (s)
0.3
0.25
0.2
0.15
0.1
0.05
0
F.
200
400
600
0
10
20
30
time (s)
0.2
0.15
0.1
0.05
0

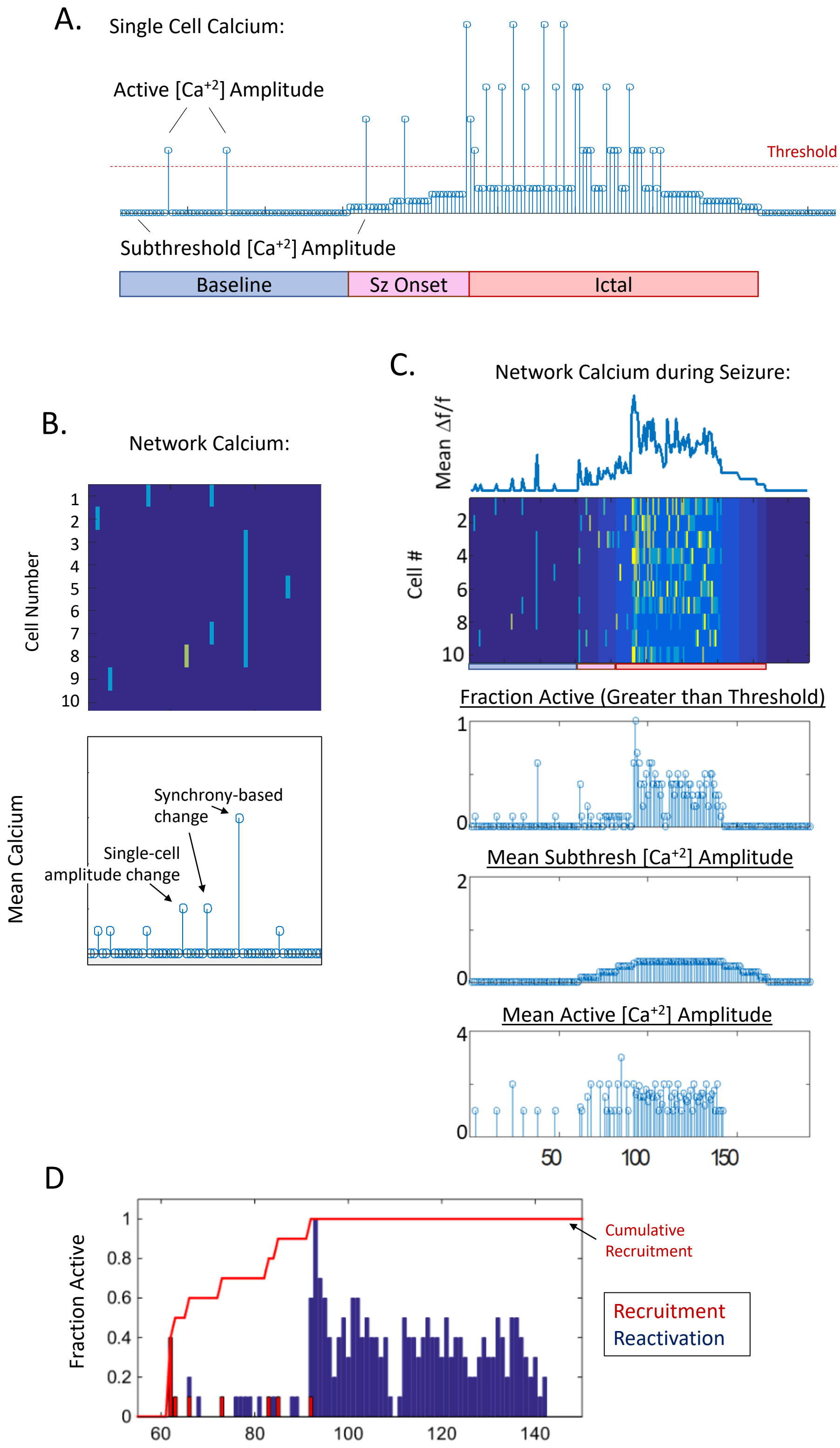
A.
Single Cell Calcium:
Active [Ca+2] Amplitude
Threshold
Subthreshold [Ca+2] Amplitude
Baseline
Sz Onset
Ictal
B.
Network Calcium:
Cell Number
1
2
3
4
5
6
7
8
9
10
Mean Calcium
Synchrony-based change
Single-cell amplitude change
C.
Network Calcium during Seizure:
Mean Δf/f
Cell #
2
4
6
8
10
Fraction Active (Greater than Threshold)
1
0
Mean Subthresh [Ca+2] Amplitude
2
0
Mean Active [Ca+2] Amplitude
4
0
50
100
150
D
Fraction Active
1
0.8
0.6
0.4
0.2
0
60
80
100
120
140
Cumulative Recruitment
Recruitment
Reactivation

In vitro - Organotypic hippocampal slice culture:

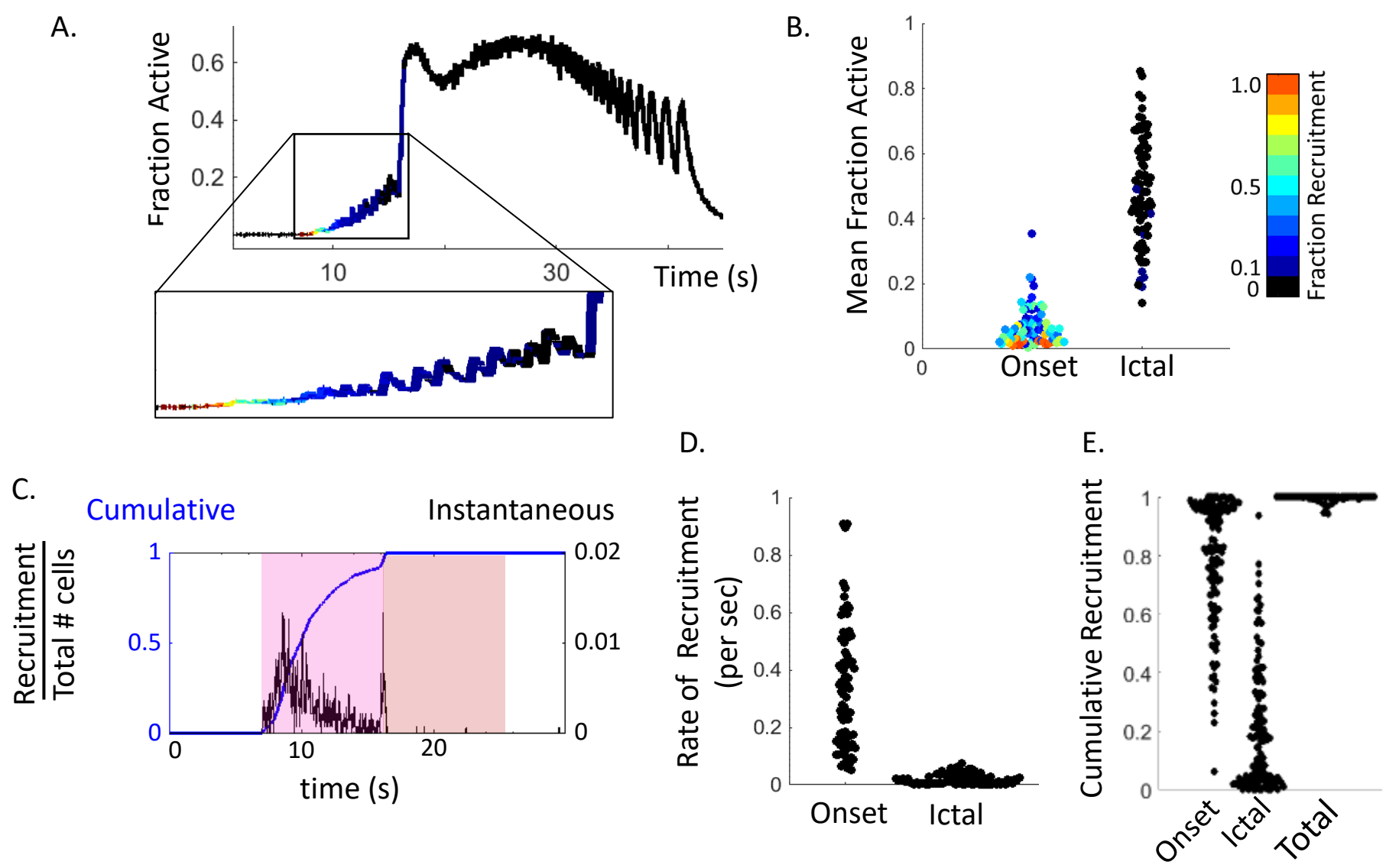

In vivo - Awake, behaving animal:

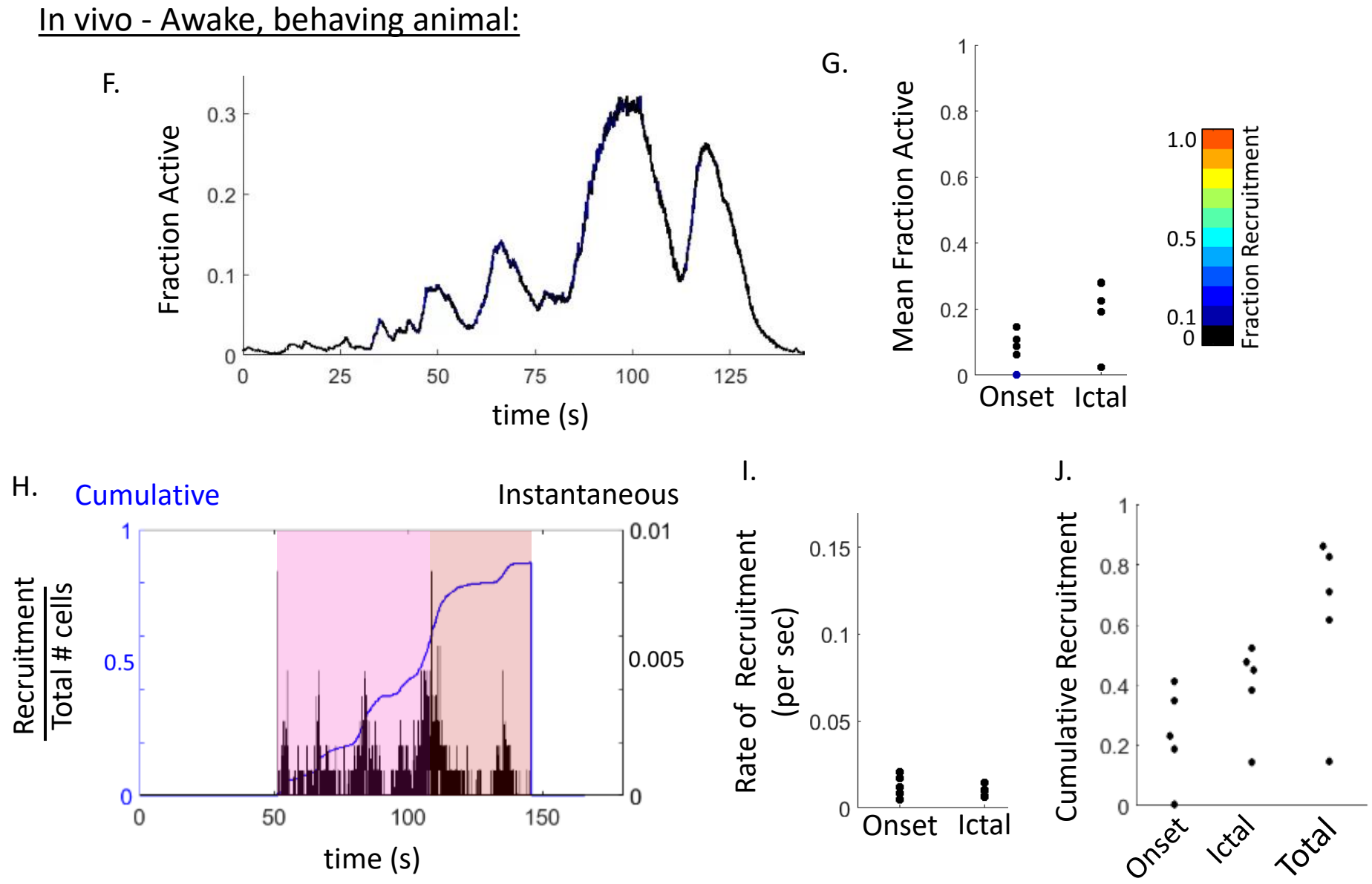

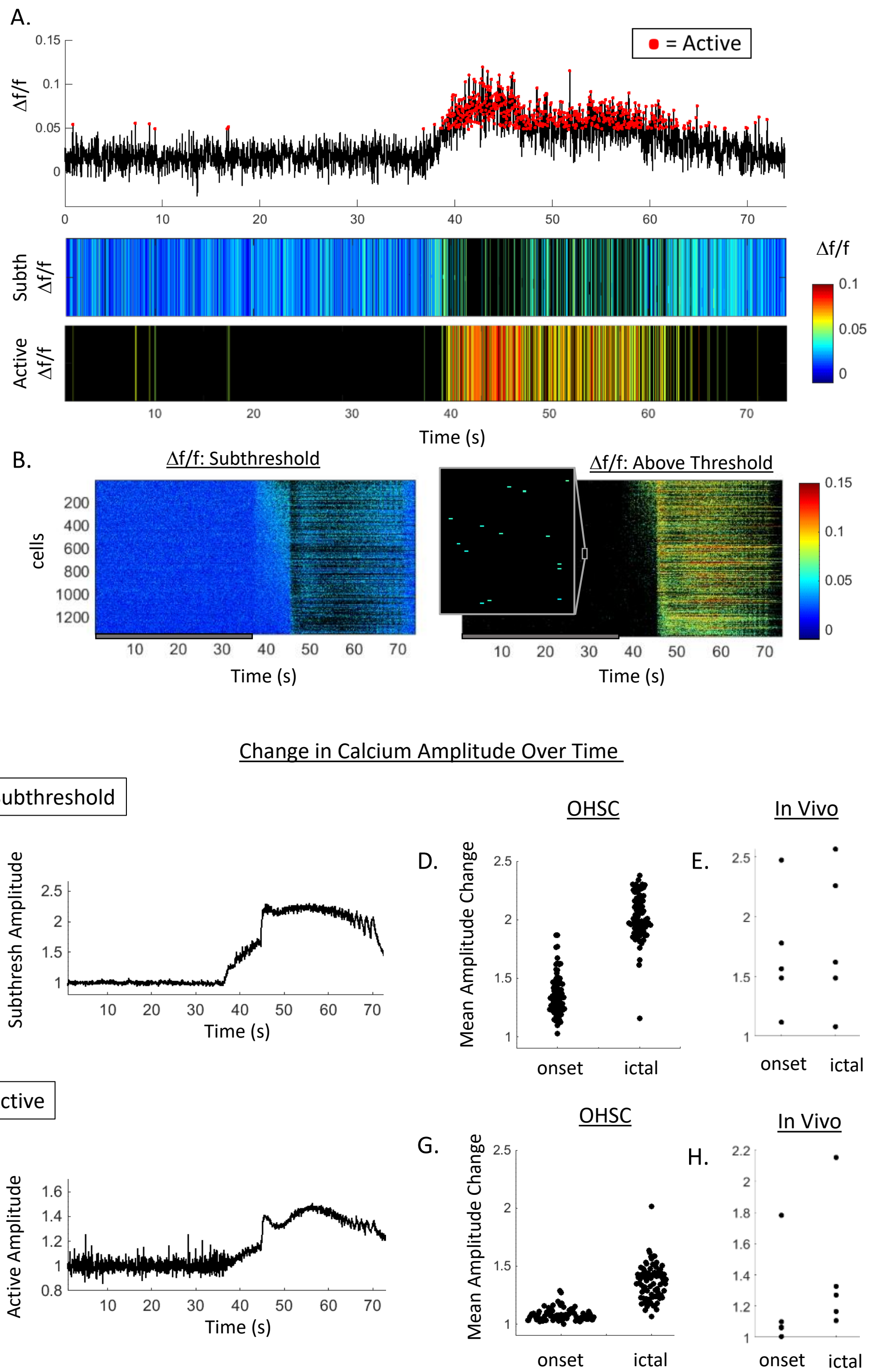
A.
= Active
Δf/f
Subth Δf/f
Active Δf/f
Time (s)
B.
Δf/f: Subthreshold
Δf/f: Above Threshold
cells
Time (s)
Change in Calcium Amplitude Over Time
Subthreshold
C.
Baseline Normalized Subthresh Amplitude
Time (s)
OHSC
In Vivo
D.
E.
Mean Amplitude Change
onset
ictal
Active
F.
Baseline Normalized Active Amplitude
Time (s)
OHSC
In Vivo
G.
H.
Mean Amplitude Change
onset
ictal

A. $$Mean\ population\ \frac{\Delta f}{f} = \underbrace{\left(Subthr[Ca^{+2}]_B * (1 - fr.act) * \frac{Subthr[Ca^{+2}]}{Subthr[Ca^{+2}]_B}\right)}_{\text{Contribution Subthreshold neurons}} + \underbrace{\left(Act[Ca^{+2}]_B * fr.act * \frac{Act[Ca^{+2}]}{Act[Ca^{+2}]_B}\right)}_{\text{Contribution Active neurons}}$$

In vitro - Organotypic hippocampal slice culture:

B.

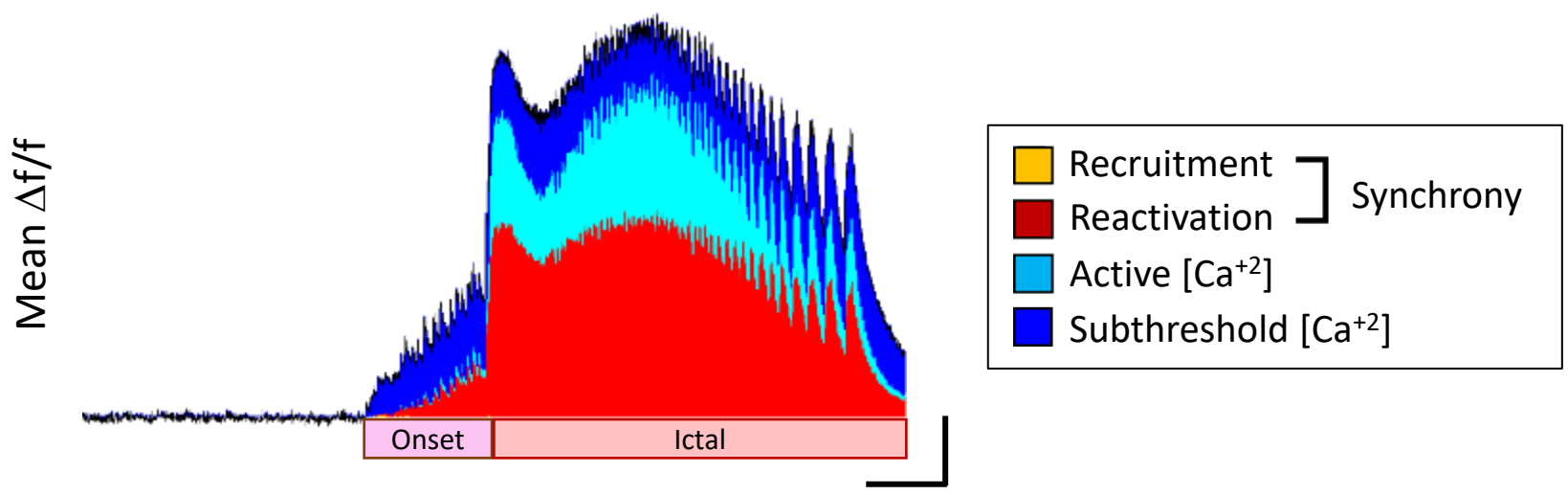

C.

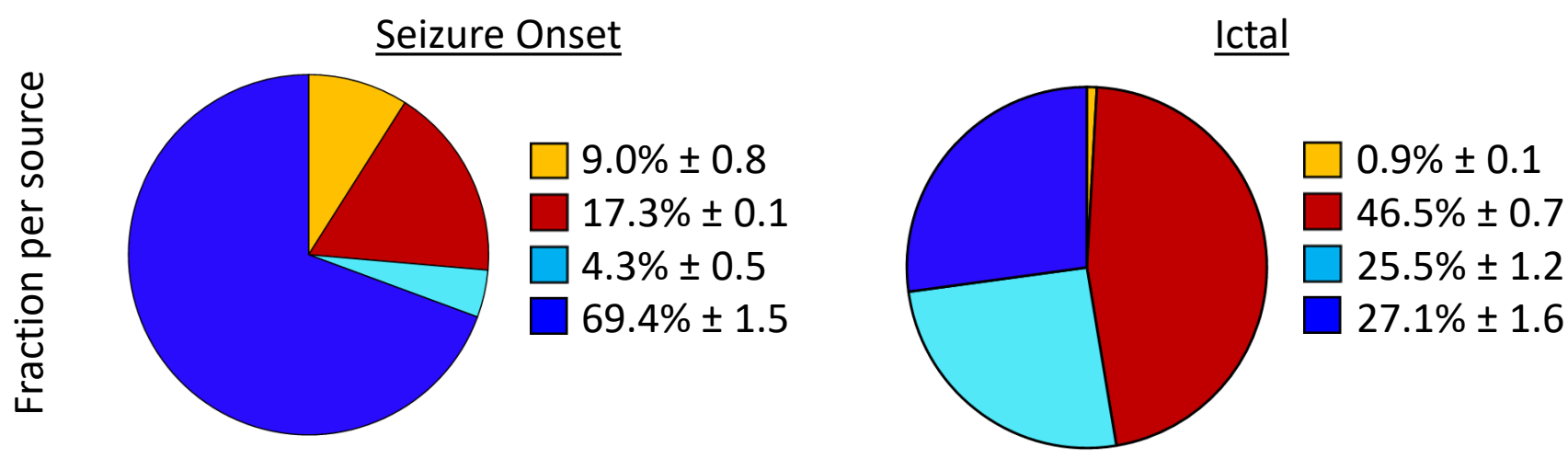

In vivo - Awake, behaving animal:

D.

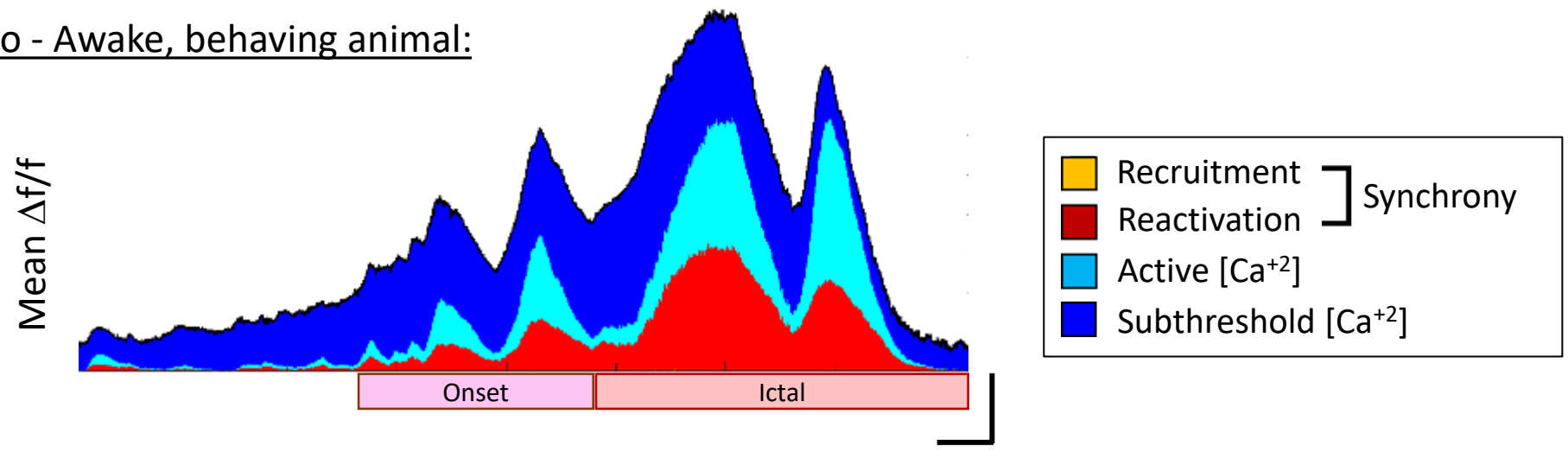
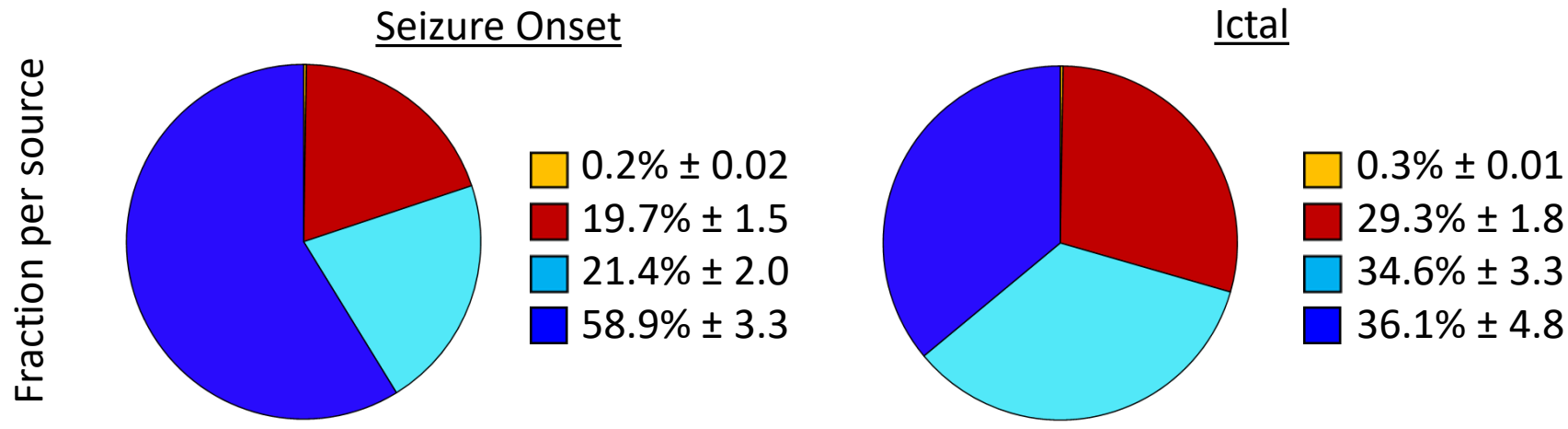
E.